Journal of Materials Science: Materials in Electronics
https://doi.org/10.1007/s10854-020-03295-w

Frequency dependence of AC conductivity and dielectric properties evaluation of in-situ prepared polyaniline/manganese dioxide composite

Yankappa A. Kulakarni[1] · M. R. Jagadeesh[2] · Sahebagouda Jambaladinni[3] · H. M. Suresh Kumar[4] · M. S. Vasanthkumar[5] · S. Shivakumara[6]

Received: 23 December 2019 / Accepted: 21 March 2020

Abstract
In the present study, polyaniline/manganese dioxide (PANI/MnO_2) nanocomposite has been synthesised by in-situ redox method. MnO_2 nanostructures are formed in PANI matrix via simple redox reaction between $KMnO_4$ and aniline monomer at ambient conditions. The composite formation, structural and morphological changes in MnO_2 and PANI/MnO_2 were characterised by Fourier transform infrared spectroscopy (FT-IR), powder X-ray diffraction (PXRD) and scanning electron microscopy (SEM) analysis. The PXRD and FT-IR patterns of the PANI/MnO_2 nanocomposites confirm the presence of α-MnO_2 nanostructures in polymer matrix. SEM images of the composite showed that MnO_2 nanostructures were dispersed uniformly in polymer matrix. AC conductivity and dielectric properties of MnO_2 nanostructures and PANI/MnO_2 nano composite were studied in the frequency range 10–100 MHz. AC conductivity of the nano composite obeyed the power law indicating the universal behaviour of disordered structures.

1 Introduction

Conducting polymers are the class of organic materials with a potential application in many technologies including energy storage [1], molecular recognition [2], electromagnetic interference shielding [3], electrochemical sensors [4] and opto-electronic devices [5]. The conducting polymers have conjugated structures consisting of an alternate single and double bonds which is one of the basic requirement for the electrical conductivity. During oxidative polymerisation process, some of the pi-bonds are broken, releasing electron which further increases their conductivity [4, 6]. The electron transport in polymeric materials has become an area of interesting research because these materials have great potential for the fabrication of solid-state devices. There are many conducting polymers including polypyrrole, polythiophene, ploy(3, 4-ethylenedioxythiophene), Polyaniline, etc., reported in literature and these polymers have been used in various applications [1, 3–5]. All these conducting polymers exhibit highly redox behaviour in the presence of heteroatom and polymer conjugation present in the respective polymer [4]. Moreover, these kind of polymers were used as electrode materials to study sensors and catalytic applications [4, 5, 7]. Among all conducting polymers, polyaniline (PANI) has attracted many researchers due to its high conductivity, unique conduction mechanism, easy preparation, simple polymerization, good thermal stability and environmental friendly impact [4, 5, 7]. PANI has been used as a conducting mediator material to contact between the atoms present in most of

✉ M. R. Jagadeesh
jmrshyagale@gmail.com

✉ S. Shivakumara
elessk@gmail.com

[1] Department of Physics, BLDEA's Vachana Pitamaha Dr. P.G. Halakatti College of Engineering and Technology, Bijapur, affiliated to Visvesvaraya Techonological University, Belgavi, Karnataka 586103, India

[2] Department of Physics, Jain Institute of Technology, Davangere, affiliated to Visvesvaraya Techonological University, Belgavi, Karnataka 577003, India

[3] Department of Physics, Government Engineering College, Huvinahadagali, Karnataka 583219, India

[4] Department of Physics, Siddaganga Institute of Technology, Tumakuru, Karnataka 572103, India

[5] Department of Physics, Acharya Institute of Technology, Soladevanahalli, Bangalore, Karnataka 560107, India

[6] Department of Chemistry, REVA University, Kattigenahalli, Yelahanka, Bangalore, Karnataka 560064, India

Published online: 06 April 2020

the semiconductor metal oxides [3, 4]. PANI has been used to enhance the electrical conductivity of metal oxide and increases overall performance of the electrode material [1, 4, 5]. There are several authors have been reported to synthesize nanocomposites using conducting polymer with metal oxide nanostructures such as ferrates, ZnO, MnO_2, SnO_2, TiO_2, etc. [7–16] to enhance the electrical conductivity of nanocomposites.

Among the available metal oxides, manganese dioxide received much attention due to its potential applications in various fields [17–20]. Manganese dioxide is cheap, abundantly available, and relatively non-toxic in nature [17–21]. MnO_2 possesses different crystallographic forms such as α-, β-, γ-, δ- and ε- type made of [MnO_6] octahedral with different connectivity. Among these crystallographic forms, α-(tunnel type structure) and δ-MnO_2 (layered type structure) are great interest and these materials have been reported for supercapacitor, sensor and battery applications [18–21]. One of the disadvantages of the manganese dioxide is poor conducting nature. The poor conducting nature of manganese dioxide can be further improved by the introduction of organic conducting matrix such as conducting polymers [21, 22]. Extensive research reports have been published in the literature to improve the conductance of manganese dioxide using conducting polymers [20–22]. The nanostructured PANI/MnO_2 composites exhibit enhanced performance compared to pure manganese oxide [22]. PANI/MnO_2 nanocomposites have been received greater interest due to low cost and environmentally friendly nature.

To the best of the author's knowledge, AC conductivity studies on PANI/MnO_2 nanocomposites are rarely reported. There are many methods available in the literature for the preparation of PANI/MnO_2 nanocomposites including chemical and electrochemical synthetic routes. In the present study, an attempt has been made to prepare PANI/MnO_2 nanocomposites by using simple reduction–oxidation reaction at ambient conditions. Herein, the simultaneous oxidation of aniline to polyaniline and reduction of $KMnO_4$ to MnO_2 (VII to IV) and as a result of this redox reaction, MnO_2 nanoparticles embedded in polyaniline matrix thus form PANI/MnO_2 nanocomposites [22]. Thus, polyaniline acts as conducting support to the poor conducting MnO_2 and further increases the performance. The resultant nanocomposite has been subjected to AC impedance spectroscopy to test the material conductivity behaviour at room temperature.

2 Experimental

2.1 Preparation of polyaniline/manganese dioxide nanostructures

All chemicals used were of analytical grade and they were used as received. In a typical preparation of polyaniline/manganese dioxide (PANI/MnO_2) nanocomposite, 3.16 g of $KMnO_4$ was dissolved in 250 mL of distilled water [7]. To the above pink-coloured solution, 1 mL of aniline monomer was added upon stirring for about 30 min. The pink-coloured solution disappears and a blackish-brown coloured precipitate was formed indicates the reduction of Mn (VII) to Mn (IV). At the same time, aniline gets oxidized to polyaniline, the obtained precipitate was washed with large amount distilled water for several times followed by ethanol. Finally, filtered and dried at 100 °C overnight. For the preparation of pure MnO_2 nanostructures, the as-prepared PANI/MnO_2 nanocomposite was heated at 600 °C for 3 h under air atmosphere. The prepared samples were used for further physicochemical characterization and electrical properties studies.

2.2 Characterization methods

Powder X-ray diffraction (XRD) patterns of the precursor and the final products were recorded using Bruker D8 advance diffractometer with monochromatized Cu Kα ($\lambda = 1.5418$ Å) incident radiation as the source. IR absorption spectrum was recorded in a FT-IR spectrum 1000 PERKIN ELMER spectrometer on dried sample using KBr pellet. Brunauer–Emmett–Teller (BET) surface area and pore size distribution of the samples were measured using Micromeritics surface area analyzer model ASAP 2020. The microscopy studies were examined by using scanning electron microscopy (SEM, FEI Co. model Sirion). AC conductivity and dielectric properties of the samples were carried out using Agilent 4294A analyser.

2.3 Preparation of electrodes and AC conductivity measurements

Room temperature AC conductivity properties of samples were examined using Agilent 4294A precision impedance analyser in the frequency range 10 Hz to 100 MHz. The voltages across the known range resistor and the DUT are measured and the impedance of the latter can be estimated. A variable frequency signal source section generates the test signals applied to the material being investigated. For impedance measurements, the samples were prepared in circular geometry with 10 mm diameter and 1 mm thickness and were coated with the silver on both sides. For

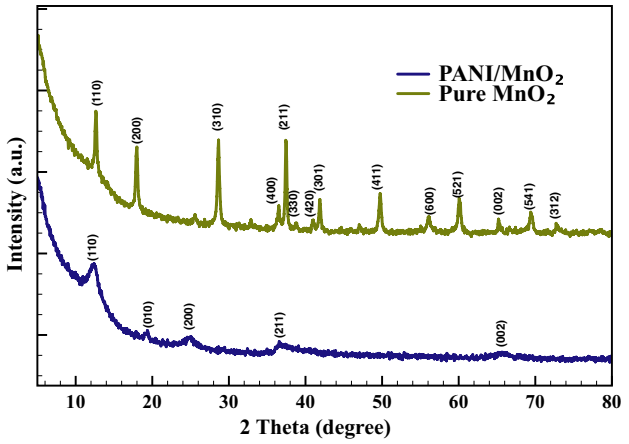

Fig. 1 XRD of PANI/MnO_2 nanocomposite and pure MnO_2 samples

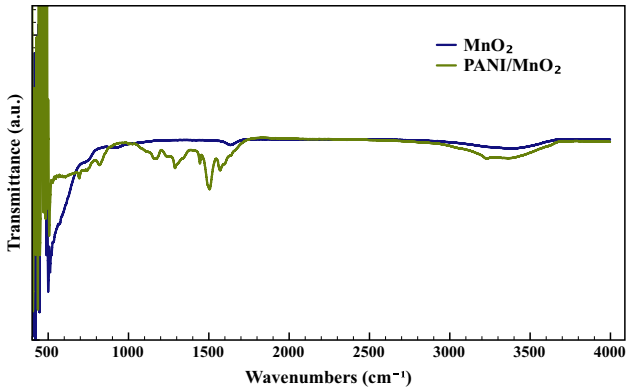

Fig. 2 FT-IR spectra of PANI/MnO_2 nanocomposite and pure MnO_2 samples

measurements, the copper wire contacts were drawn from the silver-coated surface using fine enamelled copper wire of grade 38 AWG (0.1 mm diameter) and conductive silver paint.

3 Results and discussion

The X-ray diffraction patterns (XRD) of the pure MnO_2 nanostructures and PANI/MnO_2 nanocomposite are shown in Fig. 1. The diffraction patterns of PANI/MnO_2 nanocomposite exhibit three broad peaks at 12.6°, 37.5° and 65.1° (2θ) corresponding to (110), (211) and (002) reflection planes of MnO_2, respectively. The two broad diffraction peaks at 19.34° and 24.9° correspond to (010) and (200) reflection planes of PANI in PANI/MnO_2 nanocomposite revealing the poor crystalline nature of the sample [18, 20, 22]. The series of diffraction peaks for pure MnO_2 at 12.7°, 18°, 37.4°, 42°, 49.8°, 56°, 60.2°, 65.3° and 69.6° degree correspond to (110), (200), (310), (211), (301), (411), (600), (521), (002) and (541) reflection planes, respectively, indexing the tetragonal structure (space group I4/m) of α-MnO_2 phase with lattice constants of $a = 9.8172$ and $c = 2.8582$ which are in good agreement with the reported values referring to JCPDS card number 44-0141 [18, 19, 22]. The diffraction peaks are sharp and intense, indicating that upon heating the PANI/MnO_2 nanocomposite sample at 600 °C under air atmosphere, the amorphous phase is converted to crystalline phase. Moreover, the PANI present in composite was removed by heating at 600 °C and hence pure form of MnO_2 was obtained at the end. The obtained samples were used for the further characterisation.

To know intermolecular interactions, the prepared samples were subjected to Fourier transform infrared spectroscopic (FT-IR) technique. The prepared PANI/MnO_2 nanocomposite and pure MnO_2 samples were recorded in the range 4000 to 450 cm^{-1} and are shown in Fig. 2. The bands at 1569, 1506, 1290 and 820 cm^{-1} of PANI are assigned to the C=C stretching vibrations of quinoid and benzenoid rings, the C–N stretching vibration and C–H out of plane bending vibrations, respectively [22]. The broad absorption band at 3380 cm^{-1} in the spectra of both materials can be assigned to the O–H stretching vibration. The absorption band at 500 cm^{-1} is ascribed to the contribution of the Mn–O vibrations that confirms the formation of MnO_2 [21, 22]. The PANI/MnO_2 nanocomposite spectrum shows all the absorption bands due to MnO_2 (500 cm^{-1}) and absorption bands due to PANI (1569, 1506, 1290 and 820 cm^{-1}) that confirms the existence of PANI in PANI/MnO_2 nanocomposite.

To evaluate the surface area and porous nature of the PANI/MnO_2 nanocomposite and MnO_2 nanostructures, N_2 adsorption–desorption isotherms were recorded (Fig. 3a). The specific surface area was calculated using the Brunauer–Emmett–Teller (BET) method from adsorption branch of isotherm in p/p^o range of 0.1–0.2. The isotherms of all samples resemble type IV isotherm with hysteresis in the p/p^o range of 0.5–0.99 [19, 20]. The adsorption–desorption loop indicates the presence of mesopores in the samples. Barrett–Joyner–Halenda (BJH) curves from desorption branch of isotherms are presented in Fig. 3b. The as-prepared PANI/MnO_2 nanocomposite exhibits pores with a pore size distribution of 9.3 nm, whereas pure MnO_2 nanostructures exhibit large pore of 35 nm. The BET surface area is 203 $m^2\ g^{-1}$ highlighting the overall formation of PANI/MnO_2 nanocomposite. For the pure MnO_2 nanostructures sample prepared at 600 °C, the surface area was found to be low (18 $m^2\ g^{-1}$) due to increased crystallinity.

Surface morphology notably influences the properties of the materials. The scanning electron micrographs (SEM) of PANI/MnO_2 nanocomposite and pure MnO_2 nanostructures are shown in Fig. 4. PANI/MnO_2 nanocomposite (Fig. 4a) is spongy in nature without clear boundary of particles. This is due to the amorphous nature of the material, which

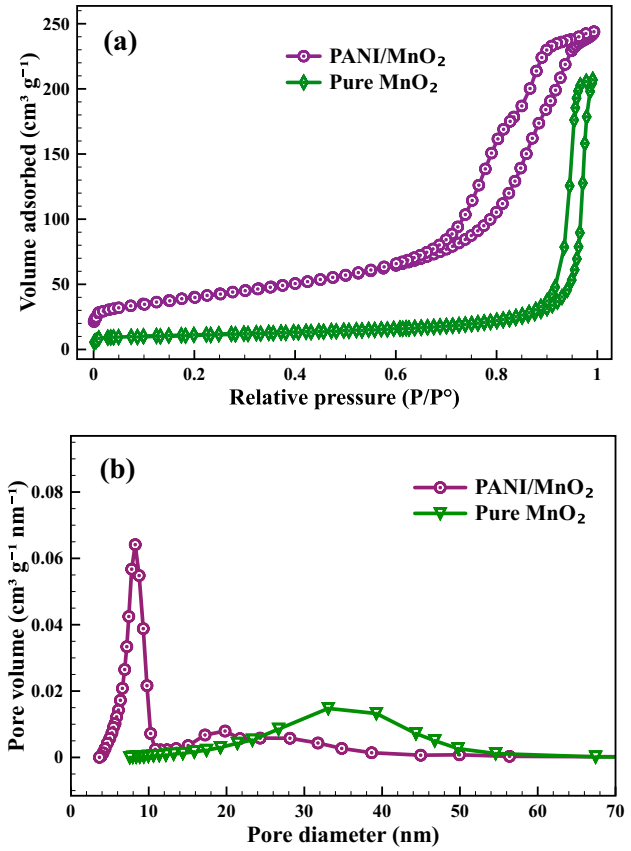

Fig. 3 N_2 adsorption–desorption, **a** BJH curves, **b** of PANI/MnO_2 nanocomposite and pure MnO_2 samples

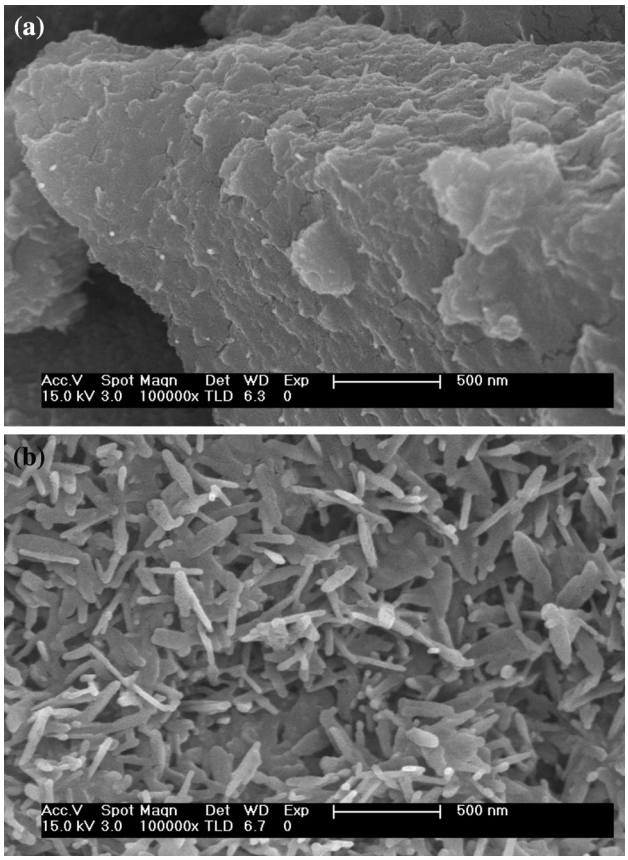

Fig. 4 Scanning electron micrographs of PANI/MnO_2 nanocomposite (**a**) and pure MnO_2 (**b**) samples

is reflected in the XRD pattern (Fig. 1). The morphology image of PANI/MnO_2 nanocomposite clearly reflects that the whole MnO_2 is covered with PANI. Upon heating at 600 °C, the morphology of PANI/MnO_2 composite interestingly changes into clear crystalline MnO_2 nanoplatelets. The morphology changes from particles to platelet nanostructures as observed in Fig. 4b.

4 Conductivity studies

Figure 5 shows the variation of AC conductivity as a function of frequency for pure MnO_2 nanostructures and PANI/MnO_2 nanocomposite. At higher frequencies, more than 80 MHz, the conductivity increases because of the contribution of polarons which are moving along shorter distances in the polymer chain. The increasing AC conductivity at higher frequencies is attributed to charge motion in the amorphous regions and this supports the presence of isolated polarons and bipolarons in this region [9–11]. It is observed from the figure that the conductivity of the PANI/MnO_2 nanocomposite and pure MnO_2 nanostructures remains constant up to 10 kHz and thereafter, the conductivity of PANI/MnO_2 nanocomposite increases

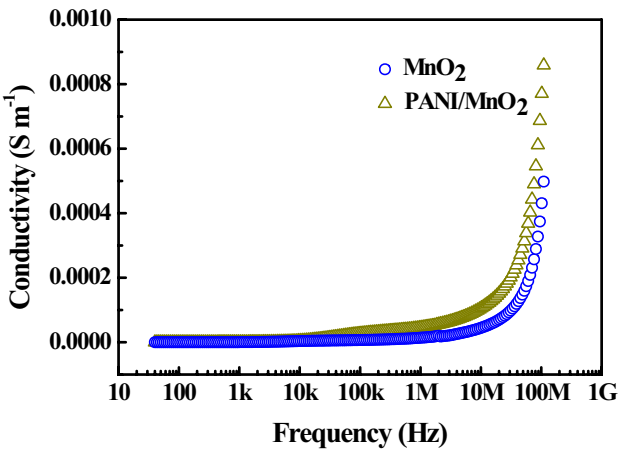

Fig. 5 AC conductivity measurement of PANI/MnO_2 nanocomposite and pure MnO_2 nanostructures

steeply, which is the characteristic feature of disordered materials. At high frequencies, AC conductivity increases due to the contribution of polarons, which are moving along smaller and smaller distances in a polymer chain [4]. Increase of AC conductivity at higher frequencies is due to the charge motion

in the amorphous region and this supports the presence of isolated polarons in this region. The high conductivity of about 0.0009 S cm^{-1} is for the sample PANI/MnO_2 nanocomposite whereas conductivity 0.0005 S cm^{-1} is observed for the pure MnO_2 nanostructures.

Figure 6 shows the variation of real part of impedance (Z') as a function of frequency varied from 50 Hz to 100 MHz at room temperature. The pattern shows the variation of Z' as a function of frequency in the low-frequency region followed by the saturation in the high-frequency region. The decrease in magnitude of Z' is with increase in frequency for both pure MnO_2 nanostructures and PANI/MnO_2. This suggests the presence of polarization behaviour in the material, such as electronic, dipolar and orientation polarization. It can be observed from the plot that conductivity of PANI/MnO_2 nano composite is more than that of pure MnO_2 nanostructures. The Z' values merge at high frequency due to the release of space charge as a result of reduction in barrier properties of the material and are responsible factor for the enhancement of AC conductivity of the PANI/MnO_2 nanocomposite material.

Figure 7 presents the variation of imaginary part of impedance (Z'') as a function of frequency. The imaginary part of impedance (Z'') decreased with increase in frequency in both the cases. The higher electrical resistance of pure MnO_2 nanostructures may be due to the absence of the PANI polymer chain. On the other hand, the electrical resistance dramatically decreased in the case of PANI/MnO_2 nanocomposite which may be due to the presence of conducting PANI polymeric chains [16]. In PANI/MnO_2, the PANI facilitating the charge carrier motion, decreases the resistance and increases conductivity.

The complex impedance analysis is another approach to predict electrical properties of the material and it is shown in Fig. 8. The resistive nature of the sample with semicircular

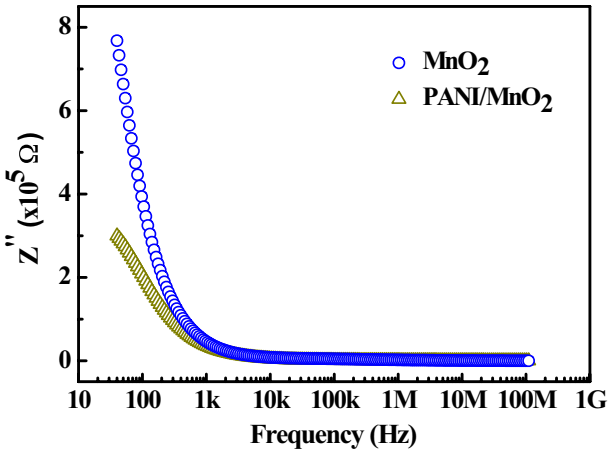

Fig. 7 Imaginary part of impedance vs frequency measurement of PANI/MnO_2 nanocomposite and pure MnO_2 nanostructures

arcs was observed. The X-axis represents the real part, while y-axis shows the imaginary part of the Nyquist plot. From these plots, it is clearly seen that the contribution of PANI in PANI/MnO_2 nanocomposites exhibit more conductivity than the pure MnO_2 nanostructures. On the other hand, the pure MnO_2 nanostructures exhibit maximum resistance than that of the PANI/MnO_2 nanocomposites which indicates that in the presence of PANI the resistivity of MnO_2 decreased and conductivity increased [21, 22].

5 Conclusions

Porous PANI/MnO_2 nanocomposite was prepared under ambient conditions. It was found that the change in morphology, crystal structure of PANI/MnO_2 nanocomposite

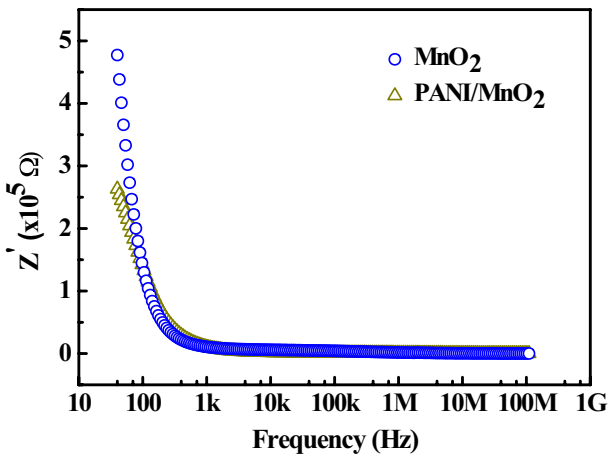

Fig. 6 Real part of impedance vs frequency measurement of PANI/MnO_2 nanocomposite, pure MnO_2 nanostructures

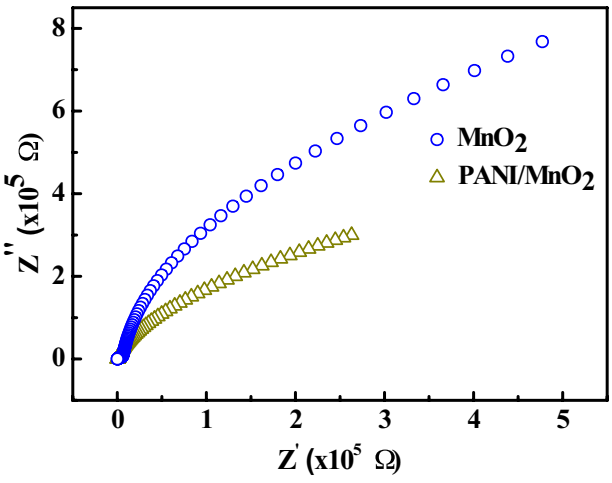

Fig. 8 Complex impedance spectra of PANI/MnO_2 nanocomposite and pure MnO_2 nanostructures

when heated at high temperature and it was converted to crystalline pure α-MnO_2. There was a notable change in the electrical properties for PANI/MnO_2 nanocomposite, and pure MnO_2 nanostructures were observed. The AC electrical conductivity of PANI/MnO_2 nanocomposite is found to be more than the pure MnO_2 and the conductivity increased as a function of increase in frequency. The high electrical conductivity of PANI/MnO_2 nanocomposite is due to the conducting polymer support to the MnO_2. As the synthesis method is simple and cost effective, the synthesis method can be used to prepare PANI/MnO_2 nanocomposite in large scale.

References

1. S. Chen, G. Meng, B. Kong, B. Xiao, Z. Wang, Z. Jing, Y. Gao, G. Wu, H. Wang, Y. Cheng, Chem. Eng. J. **387**, 123662 (2020)
2. W. Wu, C. Yu, J. Chen, Q. Yang, Int. J. Environ. Anal. Chem. **100**, 324–332 (2019)
3. A. Feng, M. Ma, Z. Jia, M. Zhang, G. Wu, RSC Adv. **9**, 25932 (2019)
4. M.H. Naveen, N.G. Gurudatt, Y.-B. Shim, Appl. Mater. Today **9**, 419–433 (2017)
5. Z. Jia, B. Wang, A. Feng, J. Liu, M. Zhang, Z. Huang, G. Wu, J. Alloys Compd. **799**, 216–223 (2019)
6. H. Khan, K. Malook, M. Shah, J. Mater. Sci. **29**, 9090–9098 (2018)
7. B.K. Sharma, A.K. Gupta, N. Khare, S. Dhawan, H. Gupta, Synth. Met. **159**, 391–395 (2009)
8. A. Vijayamari, K. Sadayandi, S. Sagadevan, P. Singh, J. Mater. Sci. **28**, 2739–2746 (2017)
9. Q. Yu, C. Wang, X. Li, Z. Li, L. Wang, Q. Zhang, G. Wu, Z. Li, Fuel **239**, 1240–1245 (2019)
10. R.E. John, A. Chandran, M. Samuel, M. Thomas, K.C. George, Physica E **116**, 113720 (2020)
11. S. Palsaniya, H.B. Nemade, A.K. Dasmahapatra, Carbon **150**, 179–190 (2019)
12. H. Khan, K. Malook, M. Shah, J. Mater. Sci. **29**, 1990–1998 (2018)
13. S. Manjunath, A.K. Koppalkar, M.V.N. Ambika Prasad, Ferroelectrics **366**, 22–28 (2008)
14. S. Manjunath, A.K. Koppalkar, M.V.N. Ambika Prasad, Ferroelectr. Lett. **35**, 36–46 (2008)
15. G.D. Prasanna, H.S. Jayanna, A.R. Lamani, M.L. Dinesha, C.S. Naveen, G.J. Shankaramurthy, Chin. Phys. Lett. **28**, 117701 (2011)
16. B.P. Prasanna, D.N. Avadhani, H.B. Muralidhara, K. Chaitra, V.R. Thomas, M. Revanasiddappa, N. Kathyayini, Bull. Mater. Sci. **39**, 667–675 (2016)
17. S. Shivakumara, T.R. Penki, N. Munichandraiah, Solid State Electrochem. **18**, 1057–1066 (2014)
18. S. Devaraj, N. Munichandraiah, J. Phys. Chem. C **112**, 4406–4417 (2008)
19. P. Ragupathy, H.N. Vasan, N. Munichandraiah, J. Electrochem. Soc. **155**, A34–A40 (2008)
20. S. Shivakumara, N. Munichandraiah, J. Alloys Compd. **787**, 1044–1050 (2019)
21. V.C. Lokhande, A.C. Lokhande, C.D. Lokhande, J.H. Kim, T. Ji, J. Alloys Compd. **682**, 381–402 (2016)
22. M.M. Mezgebe, K. Xu, G. Wei, S. Guang, H. Xu, J. Alloys Compd. **794**, 634–644 (2019)